International Conference on Control, Engineering & Information Technology (CEIT'14)
Proceedings - Copyright IPCO-2014, ISSN 2356-5608, pp.159-166

FPGA-based Sensor Fault Detection and Isolation for DTC Induction Motor based Electric Vehicle using XSG

Ferchichi Ammar, Berriri Hanen
Research Unit, Study of Industrial Systems and Renewable Energy (ESIER)
Department of Electrical Engineering, of The National Engineering School of Monastir (ENIM), Tunisia,
ferchichiomar@yahoo.fr, hanenberriri@yahoo.fr

Gdaim Soufien, Mimouni Mohamed Faouzi
Research Unit, Study of Industrial Systems and Renewable Energy (ESIER)
Department of Electrical Engineering, of The National Engineering School of Monastir (ENIM), Tunisia,
sgdaim@yahoo.fr, mfaouzi.mimouni@enim.rnu.tn

***Abstract*—** This paper deals with field programmable gate array implementation of sensor fault detection and isolation in direct torque control induction motor based electric vehicle using Xilinx System Generator. The adopted control requires the use of two current sensors. Performances and robustness of the powertrain control depend intensely on their outputs. Thus, to ensure continuous operating with reconfiguration control, a fast sensor fault detection and isolation is required. The main interest of field programmable gate array is the extremely fast computation capabilities. That allows a fast residual generation when sensor fault occurs. Using of blockset Xilinx System Generator in Matlab / Simulink allow the real-time simulation and implemented on a field programmable gate array chip without any VHSIC Hardware Description Language coding. The sensor fault detection and isolation algorithm was implemented targeting a Virtex5.

Keywords*— *FPGA; SFDI; DTC; VE; XSG;

I. INTRODUCTION

Electric vehicles (EV) currently represent a possible alternative to conventional vehicles. These last has the following great advantages for the realization of high-performance traction control. The ICV (Internal Combustion engine Vehicles) needs additional costly hardware, throttle and brake actuators but the EV does not need anything more. Traction control can be realized only by software.

The actual response of EV is quicker than an ICV because an additional delay in the mechanical system must be included. In contrast, the response time of the electric motor torque is less than 10 ms. The generated torque of electric motors can be controlled much more quickly and precisely than that of internal combustion engines. Many studies are conducted to improve the performance of all electrical vehicles; these studies concerns the technology of electric motors, power units, and the control laws respecting the autonomy between these items [1], [2], [3], [4].

Electric drivetrain includes battery, power electronics, electric motor and gearbox [2]. The asynchronous motor seems to be the best solution for electric vehicle traction. It can run on a wide range of variation of speed with low torque ripple when combined with an adequate control [1], [4]. Techniques to drive the induction motor control are discussed in the literature. The best known is the vector control is now used for electric vehicle applications [2], [3], [4], [5]. A new concept called Direct Torque Control (DTC) appeared to be competitive with vector control techniques. DTC is applied to the transitional regime and allows for better dynamic performance. For this, the DTC seems to be very suitable for electric vehicle applications [1], [6].

The electric vehicle is a key application where the propulsion control depends on the availability and the quality of sensor measurements. However, these latter are dynamic transfer elements for which only the output variable measurement is available. The real physical input is often unknown. The required sensors are current, voltage, and speed sensors. These components are usually subjected to errors such as offset, drift, disconnections and noise,. These failures obviously lead to overall EV performance deterioration [4], [7].

To improve the reliability of the electric vehicle, it is therefore compulsory to have a Sensor Fault Detection and Isolation (SFDI) system. A fault detection is one means that faulty behavior symptoms have been detected, while isolation amounts to identify the precise fault configuration leading to these symptoms [8], [9]. Several approaches have been developed based on the generation of a fault indicator called residual. Among which we find estimators [10], [6] and observers [11], [12], these two methods require a thorough knowledge of the system. An accurate model requires a relatively long time to adapt and adjust FDI algorithm for a specific application [9]. This paper interest to parity space technique, taking advantage of a share of specifications of electrical systems and secondly, equipment numerical implementation and control software [8], [13].

The control law and the diagnostic technique developed for a specific electrical system will be more reliable with the use of Field Programmable Gate Array (FPGA) because of their rapidity and parallel operation [14]. Electronic Design Automation (EDA) tools are used to generate the FPGA

configuration file called bit-stream, from a high-level description. Development of FPGA application of EDA tools used a schematic editor (in our case XSG) or an HD, (Hardware Description Language) [15]. The proposed model is made with Xilinx System Generator (XSG) and therefore requires no HDL (Hardware Description Language) programming skills, since the FPGA code is automatically generated from a Simulink block diagram. This enables the engineer to quickly modify the motor drive model at will, without any dependency on an FPGA specialist [14], [16], [17], [18].

In this paper, one of efficient technologies for designing digital systems was used, we mean Xilinx ISE suite design environment that including "Xilinx system generator" used to design and implement (DTC+SFDI). The design will be tested in a closed loop with the electromechanical drive being modeled with Simulink blockset. First, the (DTC with SFDI) are described. Next, the design procedure using XSG is presented to illustrate the important steps. Finally simulation results and discussion are given..

II. SYSTEM OVERVIEW

A. *Presentation*

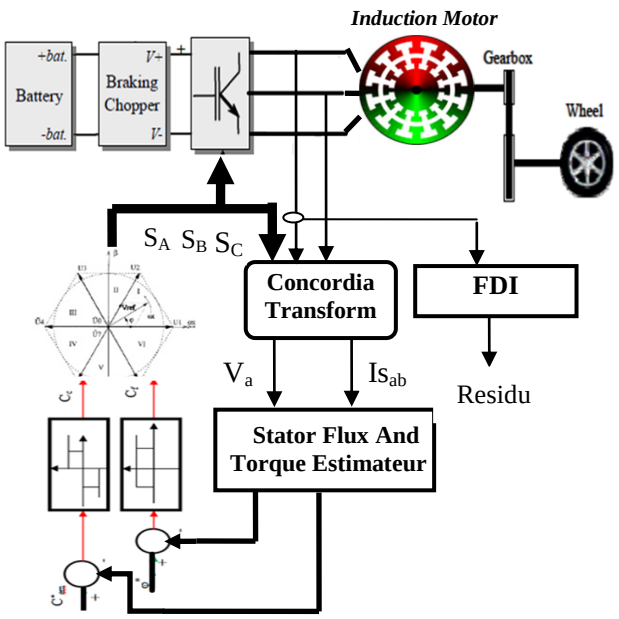

Fig. 1. Overview of sensors location in a DTC-based induction motor in EV

The basic idea of the method is to calculate flux and torque instantaneous values only from the stator variables. Flux, torque are estimated. The input of the motor controller is the reference torque (even we can apply the reference the speed, which is directly applied by the pedal of the vehicle). Control is carried out by hysteresis comparators and a switching logic table selecting the appropriate voltage inverter switching configurations [1], [6], [17], [19].

Figure 1 gives the global configuration of a DTC scheme and also shows how the EV dynamics is taken into account. To monitor the system, technical fault detection and isolation (FDI) based on parity space that allows generating a fault indicator residue through which one can decide whether the system is abnormal or not used.

B. *Direct torque control (DTC)*

Direct torque control of AC drives is based on stator voltage control; hysteresis torque and flux controllers determine the errors which govern the selection of the required voltage space vectors to be applied to the motor. A simple switching logic is used to either increase or decrease the flux, and increase or decrease the torque, or effect no changes.

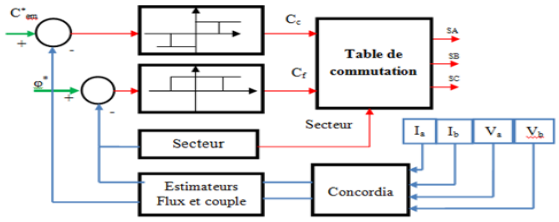

Fig. 2. Structure of the DTC

Transformation of Concordia: To swing a three-phase system to a two-phase system, the Concordia processing allowing power conservation is used.
On applying this transformation, the components of the current $(i_{s\alpha}, i_{s\beta})$ are as follows:

$$i_{s\alpha} = \sqrt{\frac{3}{2}} i_{\alpha}$$
$$i_{s\beta} = \frac{1}{\sqrt{2}}(i_b - i_c) \quad (1)$$

$$I_s = i_{s\alpha} + j.i_{s\beta} \quad (2)$$

Components of the voltage vector are reconstructed from the inverter input voltage U0, state control switches (SA SB SC) and applying the transformation CONCORDIA:

$$v_{s\alpha} = \sqrt{\frac{2}{3}} U_0 \left[S_A - \frac{1}{2}(S_B + S_C) \right]$$
$$v_{s\beta} = \sqrt{\frac{1}{2}} U_0 \left[(S_B - S_C) \right] \quad (3)$$

$$V_s = v_{s\alpha} + j\, v_{s\beta} \quad (4)$$

Flux estimator: The DTC is based on an estimation of the stator flux of the machine. The voltage to the stator is defined by:

$$\bar{v}_s = R_s . \bar{i}_s + \frac{d\bar{\phi}_s}{dt} \quad (5)$$

From this expression, the stator flux can be obtained by simple integration:

$$\bar{\varphi}_S = \int (\bar{v}_S - R_S . \bar{i}_S) dt \tag{6}$$

$$\varphi_{s\alpha} = \int (V_{S\alpha} - R_S . i_{S\alpha}) dt$$

$$\varphi_{s\beta} = \int (V_{S\beta} - R_S . i_{S\beta}) dt \tag{7}$$

The modulus of the stator flux is:

$$\varphi_S = \sqrt{\varphi_{S\alpha}^2 + \varphi_{S\beta}^2} \tag{8}$$

The result of the difference between the estimated value stream and the reference will be used by a hysteresis comparator in two levels which its output is Boolean:

- $C_f = 0$: Decrease in the flow.
- $C_f = 1$: Increase in the flow.

Torque estimator: The torque is estimated from the quantities stator current, it is flew by the following relationship:

$$C_{em} = p\left(\varphi_{S\alpha} . i_{S\beta} - \varphi_{S\beta} . i_{S\alpha}\right) \tag{9}$$

The result of the difference between the estimated torque and the reference torque will be used by a hysteresis comparator three level which its output is Boolean:

- $C_c = 1$: Increase in the torque
- $C_c = 0$: Maintain the torque
- $C_c = -1$: Decrease in the flow

Switching table: Based on the approach of Takahashi, we obtain the following table:

TABLE I. LOCATION FOR SETTING THE TORQUE AND FLUX

N		1	2	3	4	5	6
C_F	C_C						
1	1	V2	V3	V4	V5	V6	V1
	0	V7	V0	V7	V0	V7	V0
	-1	V_6	V_1	V_2	V_3	V_4	V_5
0	1	V_3	V_4	V_5	V_6	V_1	V_2
	0	V_0	V_7	V_0	V_7	V_0	V_7
	-1	V_5	V_6	V_1	V_2	V_3	V_4

V_i are given by the following relationship:

$$\bar{v}_S = v_{s\alpha} + j v_{s\beta} = \sqrt{\frac{2}{3}}(v_1 + v_2 \exp(j\frac{2\pi}{3}) + v_3 \exp(j\frac{2\pi}{3}))$$
$$\bar{v}_S = v_{s\alpha} + j v_{s\beta} = \sqrt{\frac{2}{3}} V_{DC} (C_1 + C_2 \exp(j\frac{2\pi}{3}) + C_3 \exp(j\frac{2\pi}{3})) \tag{10}$$

C. Fault Detection and Isolation (FDI)

The parity space (PS) approach is adopted here for current sensor fault detection and isolation in DTC-induction motor based EV. This approach requires generating dynamic redundancy equations for residual calculation [8], [13] and [20]. A brief description is given here based on the discrete state space model expressed by (11).

$$\begin{aligned} x(k+1) &= Ax(k) + Bu(k) \\ y(k) &= Cx(k) + Fm(k) \end{aligned} \tag{11}$$

Where x denotes n-dimensional state vector, u the m-dimensional inputs vector, y the p-dimensional measured outputs vector, m the q-dimensional fault vector to be detected. Matrices A, B, C and F are known discrete matrices of appropriate dimensions that depend on system parameters. k corresponds to the time kTa, where Ta is the sampling period of measurement. Writing (11) for each of kTa , $(k+1)Ta$ .... and $(k+s)Ta$ instants, the obtained equations are arranged by grouping known inputs and outputs in one side and state variable and faults, which are unknown variables, in the other side. Equation (12) is then derived, which links sensor outputs and sensor inputs measured on the time-window [k, k+s], using temporal redundancy.

$$Y(k,s) - G(s) \cdot U(k,s) = H(s) \cdot x(k) + H_F(s) \cdot M(k,s) \tag{12}$$

's' is the order of parity space, matrices G, H and H_F are detailed in [8].

PS approach consist of eliminating the unknown system states included in vector $x(k)$, using a projection technique. A vector Vp, called parity vector [18], [20], [21], is determined verifying (13). Multiplying each part of (12) by Vp leads to the parity equations (14) and (15). These defined such as residual. The real time implementation of the residual is performed using (15) since it is expressed using only known input and output.

$$V_p . H = 0 \tag{13}$$

$$P(k) = V_p \cdot \left[H_F(s) \cdot M(k,s)\right] \tag{14}$$

$$P(k) = V_p \cdot \left[Y(k,s) - G(s) \cdot U(k,s)\right] \tag{15}$$

The residual is null under healthy conditions and no null otherwise. Nevertheless, in real healthy conditions, there is no sensor fault but noise exists. So, the noise presence leads to a non null residual value. An accepted level of noise is used to calibrate the residual threshold.

Based on simplifications introduced by real-time considerations, application of PS approach for electrical drives allows a simple and fast SFDI algorithm [8]. Generated residual depends only on consider sensor output. Thus, it does not require the knowledge of the system model and is therefore independent from system model complexity or accuracy. Note that δ_k a difference between two consecutive measurements as detailed in (16), residual is defined by (17).

$$\delta_k = y_k - y_{k-1} \tag{16}$$

$$R_k = |\delta_k - \delta_{k-1}| + |\delta_{k-1} - \delta_{k-2}| + |\delta_{k-2} - \delta_{k-3}| \tag{17}$$

Threshold ε is defined greater than the maximum residual values $R_{k\max}$ in healthy sensor operating mode. Thus, residual $R_{k\max}$ is accurately defined. It is depends of the measured signal waveform [8], [22]. Then, in the case of sinusoidal waveform variable is given by (18).

$$R_m = 3A_m \omega^2 T_a^2 \tag{18}$$

Where Am is the maximum amplitude and $\omega = 2.\pi/\tau_\sigma$, τ_σ is the system time constant. It is very high with respect to sampling time Ta ($T_a << \tau_\sigma$).

In real situation, noise level should be added to this maximum

value of residual R_k, but anyway it remains low.

Mode of failure, the maximum residual value depends on the nature of a fault.

Offset fault: $$R'_m = R_m + 2 \times d \quad (19)$$

Gain fault: $$R'_m = R_m + 2 * (g - 1) * y_{max} \quad (20)$$

III. PROTOTYPING IN XSG

A. Introducing XSG

The control of mechatronic systems, composed of components of different nature such as power converter, electrical machine and control system. The use of advanced control algorithms ensuring good profitability and operating efficiency, depends upon being able to perform complex calculations within timing constraints can resolved with FPGAs as multiple operations are executed in parallel.

Xilinx System Generator (XSG) a high-level tool for designing high-performance DSP systems under Simulink environment, It is a highly desirable to have this simulation tool that can easily make the direct translation into hardware of control algorithms with no-knowledge of any Hardware Description Language (HDL).

XSG is a toolbox developed by Xilinx and built-in Matlab-Simulink. The models created are displayed as blocks that can be connected to the toolbox of Matlab/Simulink . Use the Xilinx Gateway blocks to interface a floating point Simulink model with a fixed-point XSG design. The Gateway-in and Gateway-out blocks, respectively, convert inputs from Simulink to XSG and outputs from XSG to Simulink. The VHDL code generated by System Genartor (SG) exactly reproduces the behavior observed in Simulink environment.

For rapid prototyping, the choice of this tool is easily explained by the advantage to simulate the control algorithm is the possibility to generate code that can be used to program an FPGA directly from the simulation model. The control system must be checked often and quickly simulated throughout the development. When the prototype is validated theoretical models on Matlab the transition to the hardware platform is fast, which makes the validation of the prototype achieved a short-term project.

The XSG tool is used to produce a model that will immediately work on the equipment when completed and validated [15], [16], [18], [23].

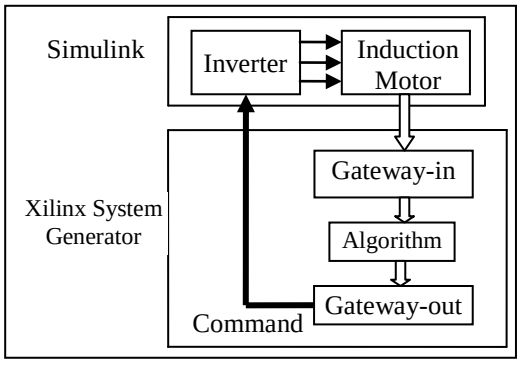

Fig. 3. Interconnection between the control system (XSG) and Power system (Simulink)

B. Modeling of FPGA-Based SFDI for DTC controller

In this section, authers explain the developpement of sensor fault detection and isolation with direct torque control induction motor based EV for FPGA implementation without any VHDL coding. Fig.4 shows overall scheme design under Matlab/simulink integrate XSG. The development of each module in terms of architecture is based on standardization principles. These principles are regularity, understandability, and reusability of already designed components [14].

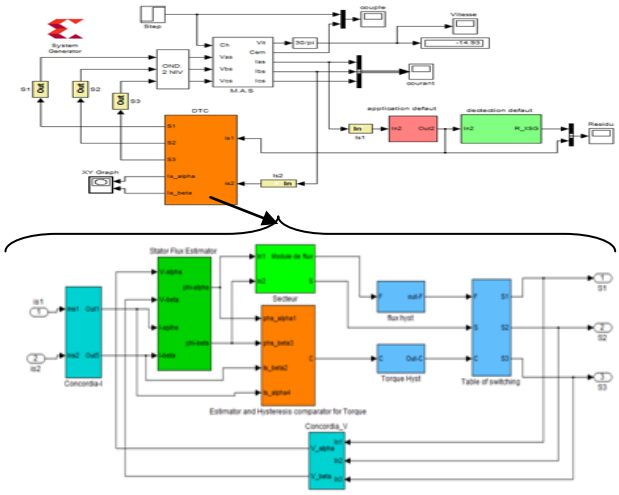

Fig. 4. SFDI for Direct Torque Control (DTC) Induction Motor

Flux estimator: The analytical expression for the flux estimator (7) shows the existence of the integral function that is not in the toolbox XSG. Then, stator flux estimator modeling based on equation (21) is designed such as Fig.5.

$$\int x dt \approx T_e \sum_{i=0}^{n} x_i \quad (21)$$

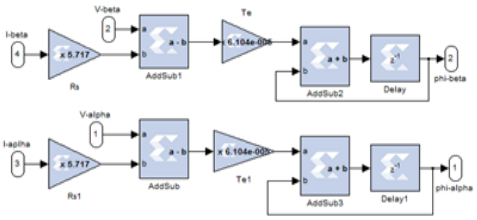

Fig. 5. Detailed block diagram stator flux estimator

Arc-tangent function: Both flow estimates are used $\varphi_{s\alpha}$ *et* $\varphi_{s\beta}$ to calculate the sector by the arc tangent function. The arc tangent function predefined into XSG has a slow execution time. That produces computation error and may affect control results. So, we defined the function arc tangent with respect a fast execution time. The proposed solution is shown in Fig. 6. It is consist of:

- Block "abs" is the real absolute value function: Function (abs) is not in the toolbox XSG as the Matlab / Simulink.
- Block "stage of calcul " contains 11 blocks.

- Block "Subsystem" represents the calculated result of the exact value of taking into account the sign of the inputs.
- The "teta" block is used to give the exact value of the angle calculated by the previous blocks in the interval [0, 2π].

Fig.6 shows a scheme of arc tangent function using XSG.

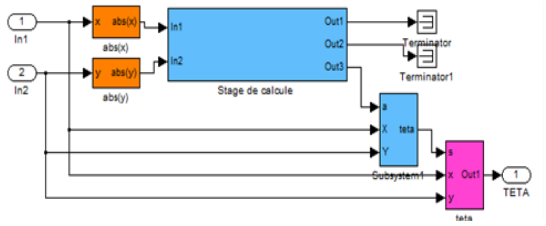

Fig. 6. Overall scheme of the arc tangent function in XSG

Hysteresis comparators: In DTC control two hysteresis comparator types are used:
Hysteresis comparator with two-level for flow control.
Hysteresis comparator with three-level for torque control.

In this case, the notion of programming in Matlab themes built in XSG by Mcode block is used. Fig. 7. (a) shows the architecture of a hysteresis comparator two levels associated with a subtraction. Fig. 7. (b) shows the architecture of *Table switching:* This is the last stage of the DTC, its basic role is to establish the three control signals to the inverter. It tests the 36 voltage vectors which are enabled by state of the input.

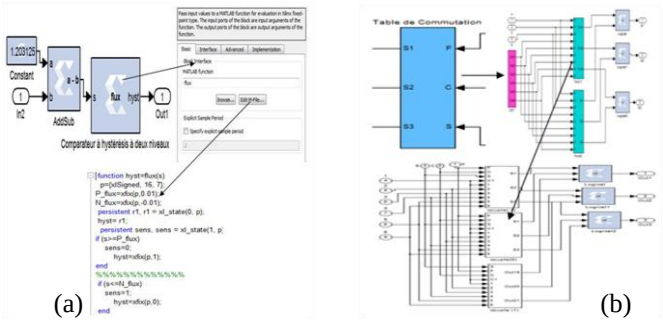

Fig. 7. (a) Architecture block «Hysteresis comparator to two levels», (b) Architecture of the block "table de commutation"

Design of fault detection and isolation in XSG: the fault detection and isolation prototype is developed in XSG like shown in Fig 8.

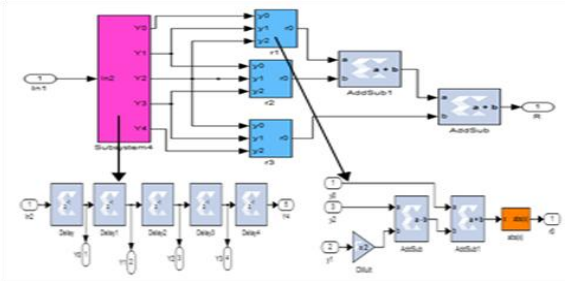

Fig. 8. Architecture FDI in XSG

IV. Simulation Results and Discussion

A. Authors and Affiliations

Simulation is then achieved under Simulink with the Xilinx System Generator (XSG) fixed-point toolbox. Fig. 4 shows a simulated version of the SFDI for DTC algorithm by XSG toolbox. The sampling frequency is fixed at 20 kHz. The obtained simulation results in healthy and faulty modes are summarized in Fig. 9, 10 and 11. The DTC strategy has been simulated on an induction motor drive, whose ratings are summarized in the Appendix.

Healthy mode

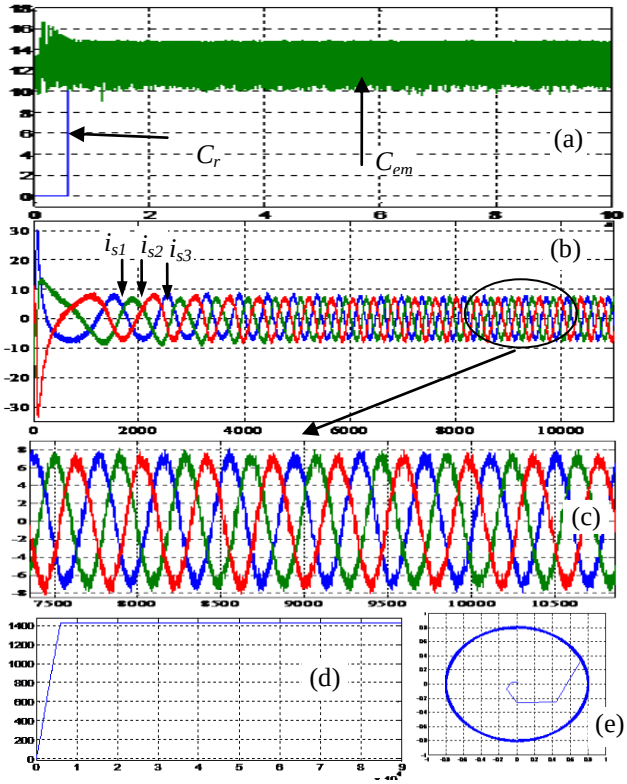

Fig. 9. Simulation DTC for induction motor: (a) Motor torque (b) Stator Current (d) Induction motor speed (c) zoom in stator current (e) Trajectory of the flux.

The simulation results of DTC for induction motor in healthy mode are shown in Fig. 9. The flux reference is 0,8 Wb. Figures illustrate both the steady state and transient performance of the proposed torque control scheme. Note that the good dynamic response of the system to a step change in torque command at t=0.3s. It is also clear in Fig. 9. (e) that the flux regulation is quite good, even during the torque transient.

Fig. 9. (a) shows an oscillatory transient increase to a maximum value of 16.5 Nm, and then it goes down almost instantly to its reference value 11 Nm with ripple amplitude in steady state. Fig. 9. (b) shows that the stator current is characterized by a high starting current up to 30 A . That allows the engine to develop a maximum power to achieve the desired speed. Then it stabilizes to its nominal value ≈ 8A as it appeared in Fig 9. (c). Figure 9. (d) shows the speed has a zero

excess, it increases rapidly with an almost linear speed up to t = 0.3 *s*, and then stabilizes around the nominal value of the motor 1440 tr / min.

Faulty mode

To evaluate the proposed SFDI for DTC strategy performance, simulations have been carried out on a induction motor in faulty mode. So, an offset fault is applied for t = 5.25*s* with an amplitude of d = 4 (50%). Fig. 10 presents a current sensor fault impacts.

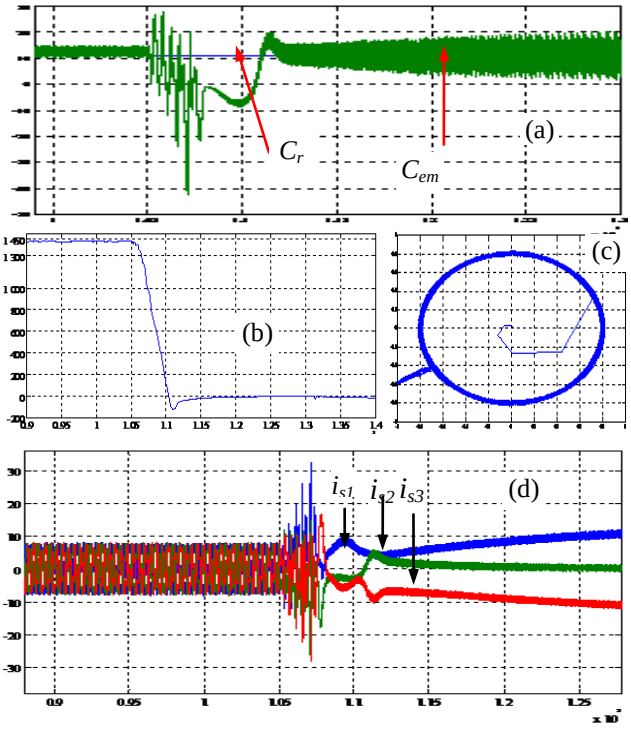

Fig. 10. Impact of offset fault on stator current sensor measurement at t=5.25s: (a) Motor torque , (b) Induction motor speed, (c) Trajectory of the flux , (d) Stator Current.

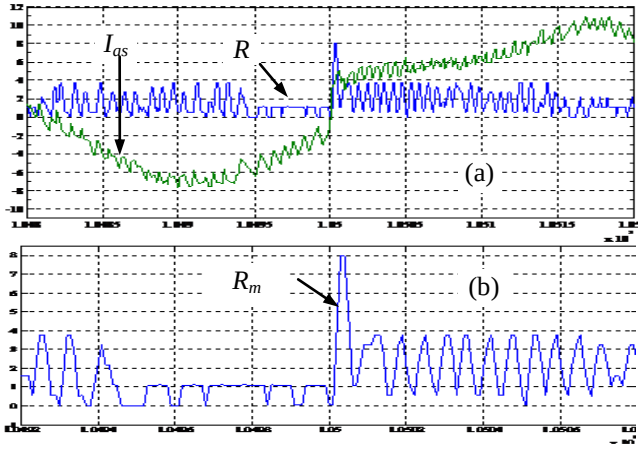

Fig. 11. Detection of offset fault on stator current sensor measurement at t=5.25s: (a) zoom in fault application, (b) Residual its zoom.

Figure 11. (a) and (b) shows that the SFDI algorithm developed in XSG has immediately detected the fault appearance. Fig 11. (a) shows stator current, an offset fault is applied at t=5.25 *s*. To emphasize residual as well in healthy condition as in faulty condition, the magnitude of applied fault is chosen little (50% of maximum magnitude). Fig 11. (b) shows that the residual value increase significantly.

High accuracy of the DTC model has been proved for the stator flux. However, any small variation in the stator flux will cause a massive starting up stator current.

The XSG is very practical since knowledge of any HDL is unnecessary; and it renders algorithm prototyping more accessible and less laborious as it permits an automatic extraction of bit-file targeting commercial FPGA devices. Figure 12 and table 2 presented an FPGA implementation of the DTC and SFDI algorithm for AC drives has been presented using the XSG tool under Simulink environment.

TABLE II. Consumed Resource report

Target Device : xc5vlx50t-3ff1136			
Logic Utilization	**Used**	**Available**	**Utilization**
Number of Slice Registers	123	28800	0 %
Number of Slice LUTs	1626	28800	5 %
Number of fully used LUT-FF pairs	41	1708	2 %
Number of bonded IOBs	52	480	10 %
Number of BUFG/BUFGCTRLs	1	32	3 %
Number of DSP48Es	14	48	29 %

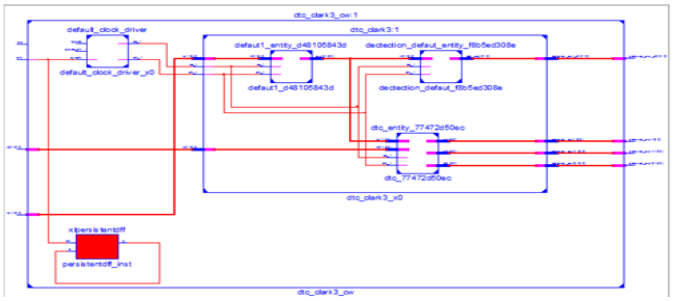

Fig. 12. RTL diagram of the FDI for DTC Induction Motor

V. CONCLUSION

This paper describes a real time simulation using Xilinx System Generator of sensor fault detection and isolation in direct torque control induction motor based electric vehicle for field programmable gate array implementation.

Simulation results demonstrate the validity and the performance of the SFDI in DTC induction motor. But we find that the contribution of clever techniques necessary to minimize the undulations at the stator flux and torque.

The method of rapid prototyping XSG enables us to develop and simulate the behavior of the machine by applying direct torque control algorithm and a sensor fault detection based on parity space. Among the advantages of XSG, it can generate a complete VHDL project to be synthesized by ISE and implemented in an FPGA. According to the synthesis results obtained by ISE HDL code generated by XSG, we see the performance of the algorithm architected speed. In terms of prospects for this work,we shall complete this work to reach a fault tolerant controler.

APPENDIX

State model of the simulated induction motor:

$$\dot{X} = [A]X + [B]U \ , \ y = [C]X$$

Where "X" is the state vector, "U" is the input vector and "y" is theoutput vector: $X = \left[i_{s\alpha} \ i_{s\beta} \ \phi_{r\alpha} \ \phi_{r\beta} \right]^T$, $U = \left[V_{s\alpha} V_{s\beta} \right]$

$$[A] = \begin{bmatrix} -\frac{R_S L_r^2 + R_r m_{sr}^2}{\sigma L_s L_r^2} & 0 & \frac{m_{sr} R_r}{\sigma L_s L_r^2} & \frac{m_{sr}}{\sigma L_s L_r}\omega \\ 0 & -\frac{R_s L_r^2 + R_r m_{sr}^2}{\sigma L_s L_r^2} & -\frac{m_{sr}}{\sigma L_s L_r}\omega & \frac{m_{sr} R_r}{\sigma L_s L_r^2} \\ \frac{R_r m_{sr}}{L_r} & 0 & -\frac{R_r}{L_r} & -\omega \\ 0 & \frac{R_r m_{sr}}{L_r} & \omega & -\frac{R_r}{L_r} \end{bmatrix}$$

$$[B] = \begin{bmatrix} \frac{1}{\sigma L_s} & 0 \\ 0 & \frac{1}{\sigma L_s} \\ 0 & 0 \\ 0 & 0 \end{bmatrix}, [C] = \begin{bmatrix} 1 & 0 & 0 & 0 \\ 0 & 1 & 0 & 0 \end{bmatrix}$$

Rated data of the simulated Induction motor

Power (KW)	Voltage (Δ/y) (V)	Pole Pair	Rs (Ω)	Rr (Ω)	Ls (H)	Lr (H)	M (H)	J (Kg.m2)	F (IS)
4	220/380	2	1.2	1.8	0.1554	0.1556	0.1500	0.024	0.011

REFERENCES

[1] Farid Khoucha, Abdelkader Khoudiri, Mohamed Benbouzid, Abdelaziz Kheloui "Commande DTC d'une propulsion moteur asynchrone / onduleur multiniveaux asymétrique pour un véhicule électrique". European Journal of Electrical Engineering, Vol. 14, pp. 237-254, (2011).

[2] Abdelfatah Nasri, Abdeldjebar Hazzab, Ismail K. Bousserhane, Samir Hadjeri, Pierre Sicard "Two Wheel Speed Robust Sliding Mode Control for Electric Vehicle Drive". Serbian journal of electrical engineering. Vol. 5, pp: 199-216, (2008).

[3] Mohamed El Hachemi Benbouzid, Demba Diallo, Mounir Zeraoulia: "Advanced Fault-Tolerant Control of Induction-Motor Drives for EV/HEV Traction Applications: From Conventional to Modern and Intelligent Control Techniques". IEEE transactions on vehicular technology, Vol. 56, pp. 519-528, (2007). doi: 10.1109/TVT.2006.889579.

[4] Demba Diallo, Mohamed El Hachemi Benbouzid, Abdessalam Makouf: "A Fault-Tolerant Control Architecture for Induction". IEEE transactions on vehicular technology, Vol. 53, pp. 1847-1855, (2004). doi: 10.1109/TVT.2004.833610.

[5] Abdelhakim Haddoun, Mohamed El Hachemi Benbouzid, Demba Diallo, Rachid Abdessemed, Jamel Ghouili, Kamel Srairi "Modeling, analysis, and neural network Control of an EV Electrical Differential". IEEE transactions on industrial electronics, Vol. 56, pp. 2286-2294, (2008). doi: 10.1109/TIE.2008.918392.

[6] Bekheira Tabbache, Mohamed Benbouzid, Abdelaziz Kheloui, Jean-Matthieu Bourgeot "DSP-Based sensor fault detection and post fault-tolerant control of an induction motor-Based electric vehicle". Hindawi Publishing Corporation International Journal of Vehicular Technology, pp. 1-7, (2012). doi:10.1155/2012/608381.

[7] Bekheïra Tabbache, Nassim Rizoug, Mohamed El Hachemi Benbouzid, Abdelaziz Kheloui "A control reconfiguration strategy for post-sensor FTC in induction motor-based EVs". IEEE transactions on vehicular technology, Vol. 62, pp. 965-971, (2013). doi: 10.1109/TVT.2012.2232325.

[8] Hanen Berriri, M.Wissem Naouar, Ilhem Slama-Belkhodja, "Parity space approach for current sensor fault detection and isolation in electrical systems. International Multi-Conference on Systems, Signals & Devices, Vol.8, pp. 1-7, (2011). doi: 10.1109/SSD.2011.5767496.

[9] Qinghua zhang, Michèle Basseville, Albert Benveniste, "Fault detection and isolation in nonlinear dynamic systems: A combined input-output and local approach". Elsevier Science Ltd, pp. 1359-1373, (1998).

[10] Kai Rothenhagen, Friedrich Wilhelm Fuchs, "Current sensor fault detection by bilinear observer for a doubly fed induction generator". IEEE transactions on Industrial Electronics, pp. 1369 – 1374, (2006). doi: 10.1109/IECON.2006.347390.

[11] Christopher Edwardsa, Chee Pin Tanb, "Sensor fault tolerant control using sliding mode observers". Elsevier Ltd: Control Engineering Practice, pp. 897–908, (2006). doi:10.1016/j.conengprac.2005.05.002.

[12] Kai Rothenhagen, Friedrich Wilhelm Fuchs, "Current sensor fault detection, isolation, and reconfiguration for doubly fed Induction Generators". IEEE transactions on Industrial Electronics, Vol. 56, pp. 4239-4245, (2009). doi: 10.1109/TIE.2009.2017562.

[13] Hanen Berriri, Mohamed Wissem Naouar, Ilhem Slama-Belkhodja: "Easy and fast sensor fault detection and isolation algorithm for electrical drives". IEEE transactions on power electronics, Vol. 27, pp. 490-499, (2012). doi: 10.1109/TPEL.2011.2140333.

[14] Francesco Ricci, Hoang Le-Huy, "Modeling and simulation of FPGA-based variable-speed drives using Simulink". Elsevier. Mathematics and Computers in Simulation, pp. 183–195, (2003), doi:10.1016/S0378-4754(03)00066-1.

[15] Stéphane Simard, Jean-Gabriel Mailloux, and Rachid Beguenane, "Prototyping advanced control systems on FPGA". Hindawi Publishing Corporation EURASIP Journal on Embedded System, pp. 1-12 pages, (2009). doi:10.1155/2009/897023.

[16] Jean-Gabriel Mailloux, Stéphane Simard, Rachid Beguenane, "FPGA implementation of Induction Motor Vector Control using Xilinx System Generator". WSEAS international conference on circuits, systems, electronics, control and signal processing, Cairo, Egypt, pp. 252-257, (2007).

[17] Francesco Ricci, Hoang Le-Huy, "An FPGA-Based Rapid Prototyping Platform For Variable-Speed Drives". IEEE Industrial Electronics Society, Vol. 2, pp. 1156 – 1161, (2002), doi: 10.1109/IECON.2002.1185436.

[18] Ozkan Akin, Irfan Alan: "The use of FPGA in field-oriented control of an induction machine". Turk J Elec Eng & Comp Sci, Vol. 18, pp. 943-962, (2010), doi: 10.3906/elk-0905-40.

[19] Bekheïra Tabbache, Mohamed El Hachemi Benbouzid, Abdelaziz Kheloui, Jean-Matthieu Bourgeot, "Virtual-Sensor-Based Maximum-Likelihood Voting Approach for Fault-Tolerant Control of Electric Vehicle Powertrain". IEEE transactions on vehicular technology, Vol. 62, pp. 1075-1083,(2013), doi: 10.1109/TVT.2012.2230200.

[20] Chun Wah Chan, Song Hua, Zhang Hong-Yue, "Application of fully decoupled parity equation in fault detection and identification of DC Motors". IEEE transactions on Industrial Electronics, Vol. 53, pp. 1277-1284, (2006), doi: 10.1109/TIE.2006.878304.

[21] Edward Y. Chow, Alan S. Willsky, "Analytical Redundancy and the Design of Robust Failure Detection Systems". IEEE transactions on automatic control, Vol. AC-29, pp. 603-614, (1984).

[22] Hanen Berriri, Mohamed Wissem Naouar, and Ilhem Slama-Belkhodja: "Sensor fault tolerant control for wind turbine systems with doubly fed induction generator". Electrimacs, Cergy-Pontoise, France, pp. 1-6, (2011).

[23] Lahcene Merah, Adda Ali-Pacha, Naima Hadj Said, Mustafa Mamat: "Design and FPGA Implementation of Lorenz Chaotic System for Information Security Issues". Applied Mathematical Sciences, Vol. 7, pp. 237 – 246, (2013).